A Mid-Infrared study of the properties of Blue Compact Dwarf galaxies using the Wide-Field Infrared Survey Explorer

D. A. Ludovici and J. Toomey
Department of Physics and Astronomy, University of Iowa, Iowa City, IA 52242

ABSTRACT

Blue Compact Dwarf galaxies are small, gas rich galaxies that are currently in a period of enhanced star formation. These galaxies are characterized by their blue color, low metallicity, and compact size and are important for our understanding of the early Universe. We examined a sample of known Blue Compact Dwarfs, determined their counterparts in the Wide-field Infrared Survey Explorer (WISE) point source catalog, and have compared their mid-infrared colors to those of other galaxies. From this analysis, we have determined criteria to be used in a search of the WISE point source catalog for new Blue Compact Dwarf candidates and have found several Blue Compact Dwarfs with WISE colors consistent with galaxies containing an active galactic nucleus.

Subject headings: galaxies:dwarf; galaxies:active; infrared:galaxies

1. Introduction

1.1. General Properties

Blue Compact Dwarf galaxies (BCDs) are considered to be the low redshift analogs to the small galaxies that were prevalent in the early Universe and are also known as Blue Amorphous Galaxies and HII galaxies (Kunth & Östlin 2000). Small primordial galaxies are thought to have coalesced to form the larger galaxies that we see today through hierarchical galaxy formation (Cairós et al. 2010). BCDs are undergoing a phase of intense star formation characterized by strong B-band emission from hot, bright O and B main sequence stars. Though BCDs have been investigated for many decades, only with the advent of modern instruments and imaging techniques are we able to investigate the detailed properties of these objects over a large sample.

BCDs show many interesting features that set them apart from other galaxies. These galaxies are typically small with an optical size of approximately 1 kpc for their star forming region. They are characterized by strong blue optical emission ($M_B \leq -18$) (Bekki 2008), as well as a large HI disk. Observations of Oxygen line spectra have yielded a range of metallicity for BCDs from $1/50Z_\odot - 1/3Z_\odot$ (Izotov & Thuan 1999). From these properties, we infer that BCDs represent small galaxies that are similar to galaxies in the early universe.

From detailed observations of BCDs, two general classes of these galaxies (active and passive) are apparent. Active BCDs are host to super star clusters and show compact star formation regions on the scale of 50 pc. In addition, active BCDs show high gas densities, large amounts of HII emission, high optical depths, and high dust temperatures (Griffith et al. 2011). The super star clusters located in active BCDs provide a useful mechanism to determine the metallicities of BCDs in the mid-infrared. Despite the low metallicity of BCDs, dust can be found throughout the star formation region (Wu et al. 2008). This dust formation is the result of Type II supernovae explosions resultant from runaway star formation (Griffith et al. 2011). In passive BCDs, star forming regions are spread out over a larger volume (at least 100 pc) and are less dense ($\rho \leq 100\,\mathrm{cm}^{-3}$) (Griffith et al. 2011). Other characteristics common to BCDs include star formation rates (SFR) of $10^{-3}\,\mathrm{M}_\odot\mathrm{yr}^{-1}$ to $1\,\mathrm{M}_\odot\mathrm{yr}^{-1}$ (Zhao et al. 2011). As this rapid

and violent star formation is episodic and periodic, BCDs will eventually cycle into a tranquil phase.

Although not present in every example, most BCDs contain a bimodal stellar distribution. A population of older stars forms a low surface brightness red background superimposed on the brighter blue from the younger stellar population.

Two predominant theories attempt to explain star formation in BCDs. The first theory details a star formation history through tidal interaction or merging with other galactic objects. The opposing gravitational forces between the two interacting objects disturb the HI discs around BCDs. This induces fluctuations in the gas disks, creating regions of higher density that can initiate a round of star formation. Encounters with other objects may occur more than once in a BCDs evolution and could result in one or more stellar populations in an individual BCD.

Sánchez Almeida et al. (2008) presents a second model for BCD star formation. They explain the bimodal stellar population with a galactic fountain model. In this model, the gas is expelled outward by powerful supernova in an initial round of star formation. Over time the ejected gas condenses and cools, at which point it accretes back onto the galaxy (Kunth & Östlin 2000). The slow gas infall reaches a critical density and triggers a new round of star formation.

Current BCD modeling predominately initiates with a progenitor dwarf having little or no SFR and containing an extended HI disc. Through its evolution BCDs form bright blue star forming regions while retaining massive HI envelops (Bekki 2008). These hydrogen rich gas clouds provide the reservoir of fuel for episodic star formation that yields low metallicity stellar populations in BCDs. The gas rich envelopes have been estimated to be as high as 30 percent of the mass of BCDs (Zhao et al. 2011).

BCDs are thought to have evolutionary links with other dwarf type galaxies, though modeling has not established clear physical connections (Bekki 2008). The stellar formation processes in BCDs are not active enough to expel their HI envelop (Bekki 2008). Because of this, they are not expected to transition into a gas-poor dwarf ellipticals. Similar to dwarf ellipticals, observations have shown that dwarf spheroidals contain little or no gas and no HII regions (Kunth & Östlin 2000). The attempts to link dwarf irregulars have been the most promising, in that BCDs are likely to evolve into gas-rich nucleated dwarf irregulars after significant fading of their blue compact cores (Bekki 2008). Dwarfs could evolve slowly due to low mass densities or because they are more susceptible to metal enriched material loss from supernova driven winds (Kunth & Östlin 2000).

1.2. Importance to Theories

Due to the low luminosities of BCDs, no high redshift counterparts to nearby BCDs have been detected. Thus, the study of nearby BCDs provide the best insight into the environment of the early galaxies.

The extremely low metallicity of most BCDs allows the study of the chemical composition of the early universe. In particular, BCDs can be used to put constraints on the primordial ${}^{4}_{2}\mathrm{He}$ abundance (Olive et al. 1990). By examining the abundances of Carbon, Nitrogen, and Oxygen, and assuming a model for the stellar synthesis of these elements compared to He, the enrichment of the ISM in the BCD can be traced (Olive et al. 1990). Since BCDs also contain gas rich clouds that have undergone little to no star formation, they offer a unique environment for studying the primordial ratio of H/He. Using this, comparisons with cosmological models can be made, and greater constraints can be put on the density parameter for matter (Olive et al. 1990). Also, the low metallicity of BCDs may permit study of metal distribution within near pristine metal poor environments.

If the theory of hierarchical galaxy formation is correct, BCD mergers may be the best local analogs to the formation of large galaxies in the early universe. At high redshift, quasars and other large galaxies show a significant dust content and higher metallicities (Kunth & Östlin 2000). This implies that the enrichment of metals in these objects from stellar nucleosynthesis occurred prior to their development. Thus, the population of large, metal rich galaxies we see in the local universe should have been formed from higher metallicity pieces. Because of this, BCDs may offer an unique glance into the history of galaxy formation.

1.3. BCDs and AGN

Although, super-massive black holes are now known to be common in large galaxies, few examples of active galactic nuclei (AGN) are found in dwarf galaxies (Filippenko & Sargent 1989; Barth et al. 2004). The recent discovery of a weak AGN in Henize 2-10 (Reines et al. 2011) complicates galactic formation models. The discovery of super-massive black holes in dwarf galaxies implies that super-massive black hole formation may precede the development of more massive galaxies. Furthermore, in support of the galactic merging concept, Henize 2-10 exhibits a tail-like structure in its stellar and gaseous distributions that was likely the result of interaction with another galaxy (Reines et al. 2011).

Because of their importance to galaxy formation models and theories explaining the early universe, we decided to investigate the mid-infrared colors of BCDs. Using these mid-infrared colors we investigate constraints which can be used to aid searches for new BCDs. In addition we examine the infrared properties of known BCDs and compare them to other galaxy types.

2. Data

Given that BCDs typically have a region of violent star formation, WISE serves as an ideal instrument in detecting the infrared (IR) radiation emitted by the surrounding ultra-violet excited dust regions. WISE can perform photometry in four bands: W1 (3.4 microns), W2 (4.6 microns), W3 (12 microns), and W4 (22 microns). These photometric bands allow determination of mid-infrared colors, while the all sky coverage of WISE permits a large number of sources to be studied.

For this analysis, we utilized the NASA Extragalactic Database (NED) to gather a sample of known BCDs. The list from NED was then checked against the literature to verify the current status of these objects as BCDs. Galaxy pairs were also excluded from analysis to prevent source confusion. The resolution of WISE is highest in W1, with a resolution of 6.1 arcsecond. We assumed that WISE point sources within half a resolution element of a catalog position would be related. Thus, the WISE point source catalog was searched for WISE sources within three arcseconds of the BCD catalog positions gathered from NED. A total of 116 WISE BCD counterparts were found in the WISE point source catalog. All of these sources were used in the analysis. In addition to the BCDs pulled from NED, we also utilized a selection of BCDs from the literature that have not yet been listed in NED. This added a total of eight additional BCD sources to our analysis (Wu et al. 2008; Griffith et al. 2011) A list of BCDs used in our study can be found in at the end of the paper in Table 3.

To compare the BCDs against a different population of galaxies, a sample of spiral galaxies was selected. Spirals were chosen due to their ongoing star formation similar to BCDs (Searle & Sargent 1972). The sample of spirals was pulled from NED. Galaxies considered for comparisons to the BCDs were constrained by limiting their redshift to $z \leq 0.025$ to prevent changes in their WISE colors due to Doppler shift. This sample was further limited by removing all galaxies with a near infrared K-band 20 magnitude isophotal diameter larger than three WISE resolution elements ($\leq$ 18.9 arcseconds) in the W1 band (6.1 arcseconds) (Wright et al. 2010). The limitation of the diameter to three WISE resolution elements assured the detection of the galaxy as a whole, as opposed to individual regions within the spiral galaxies. Counterparts within three arcseconds in the WISE point source catalog were selected giving a sample of 481 spiral galaxies.

3. Analysis and Results

For each of the galaxies, WISE photometry for W1, W2, W3, and W4 was gathered. Using the four photometric bands, six WISE photometric colors were determined. These colors were then plotted in 20 distinct three dimensional combinations to compare the WISE colors of spirals and BCDs. Each of these combinations was analyzed to examine the variation in WISE colors for the galaxies. For ease of viewing in the printed literature, two dimensional plots were also created.

Many of the color-color diagrams show similar trends. A sample of typical color-color diagrams are shown in Figure 1 which demonstrate the trends we typically see in the rest of the data. In some color combinations, strong correlations between the BCDs and spirals are seen (Figure

1 Top). While in others, BCDs show a clear offset from normal spiral galaxies (Figure 1 Middle and Bottom). In most cases, a significant spread in WISE mid-infrared colors is seen for all sources.

4. Conclusions

4.1. BCD Color Constraints

From our analysis, we can see that BCDs and spirals do have significant overlap in WISE colors. However, though we can not completely separate the galaxies, we are able to draw some conclusions to help narrow searches for BCDs. When viewing the three dimensional color-color diagrams (Figure 2), we can see that most BCDs and spirals lie along plane in the WISE colors with only a few BCDs with very red colors diverging from this trend. The middle plot in Figure 1 demonstrates that, with the exception of two outliers, no BCDs can be seen with a [W3-W4] color less than 2.6. Additionally, as is shown in the bottom plot of Figure 1, no BCDs are found in a region above a line in [W1-W3] vs. [W1-W4] . Using all of our color-color comparisons we developed several criteria to filter known BCDs from spiral galaxies. Two modes of selection criteria were established; the first, solely based on a single color and second being a sloped line that followed the prevailing position of BCDs along the diagram. Our color criteria can be seen in Table 1.

After developing this criteria, it was applied to the WISE catalog. As an initial test, a 15 arcmin sample in the WISE catalog was taken centered on the location of BCD candidate CG 0563 (Wu et al. 2008). The WISE point source catalog contained 2290 sources in this region. Of these sources, a total of 49 were found to have been detected in all four color bands and met our selection criteria (including BCD candidate CG 0563). This represents approximately two percent of the cataloged point sources. With the completion of this test, our same criteria were applied to the entire WISE catalog with the additional constraint that galactic latitudes $l \leq |10°|$ be excluded to remove the zone of avoidance. In addition, we limited ourselves to sources with a signal to noise ratio of greater than four. The output resulted in approximately six-hundred thousand sources. This represents about 0.1% of the total WISE cataloged point sources. Using these constraints, the WISE

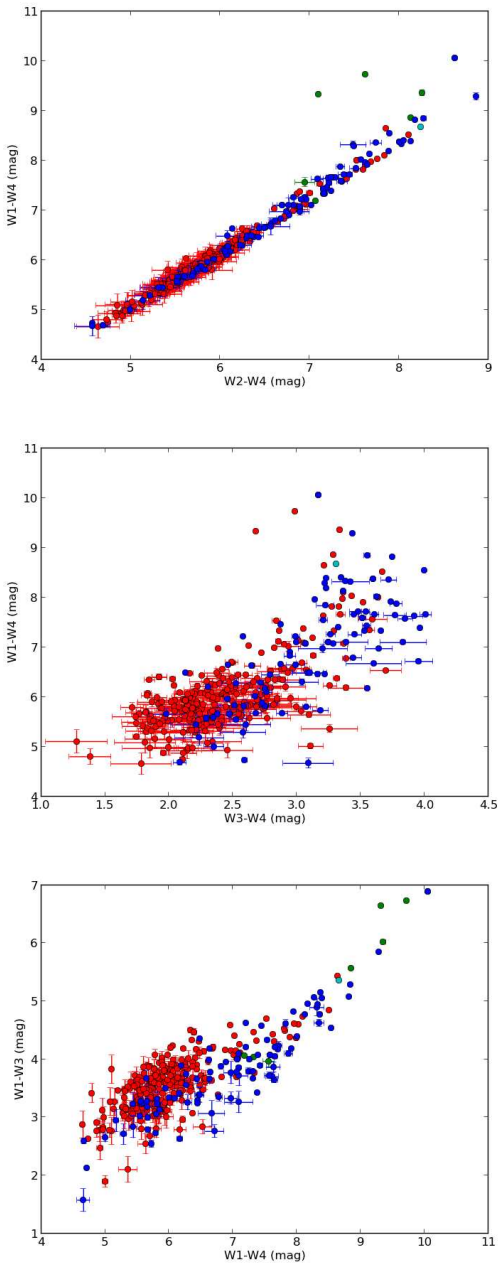

Fig. 1.— Top: WISE [W2-W4] vs. [W1-W4] Middle: [W1-W4] vs. [W3-W4] Bottom: [W1-W3] vs. [W1-W4] color comparison of spiral galaxies (red dots) and BCDs; blue dots (NED), cyan dot (He 2-10 (Reines et al. 2011), green dots (Wu et al. 2008; Griffith et al. 2011)

points source catalog becomes a viable source of new BCD candidates. This would allow targeted searches for BCDs, thus eliminating the need for blind surveys. Using WISE BCD candidates, targeted optical surveys could examine candidates $[B-V]$ color to check for consistency with known BCDs ($[B-V] \geq 0.3$). By combining WISE data with an all sky optical survey, it would be quite feasible to conduct a search for new BCD galaxies.

Table 1:
BCD Color Criteria

$-0.1 \leq [W1-W2] \leq 0.5$
$1.9 \leq [W2-W3] \leq 4.5$
$2.2 \leq [W3-W4] \leq 4.1$
$4.0 \leq [W2-W4] \leq 8.3$
$2.1 \leq [W1-W3] \leq 4.8$
$4.6 \leq [W1-W4] \leq 8.5$
$[W1-W3] \leq 1.04[W1-W4] - 2.5$
$[W1-W3] \leq 1.23[W2-W4] - 3.45$
$[W1-W4] \geq 1.10[W2-W3] + 1.95$
$[W1-W4] \geq 1.91[W2-W3] - 0.71$

4.2. Candidate AGN BCDs

One striking feature in our WISE color analysis are the BCDs with very red WISE colors. Overplotting our BCD colors onto the expected WISE colors taken from Figure 12 of Wright et al. (2010), it can be seen that these galaxies are not coincident with quiescent galaxies (Figure 3).

These few BCDs show WISE colors consistent with Ultra-Luminous Infrared Galaxies (ULIRGS), Luminous Infrared Galaxies (LIRGs), Low-Ionization Nuclear Emission-line Region Galaxies (LINERS), Starburst Galaxies, and Galaxies with obscured AGN. To investigate the relationship of these galaxies to the one BCD known to possess an AGN (He 2-10), we have marked it in green on our figures. As can be clearly seen, He 2-10 lies outside of the normal range for spiral galaxies lying clearly in red WISE colors occupied by active galaxies. Because of this, we conclude that these BCDs possessing $[W1-W2] \geq 0.5$ or $[W2-W3] \geq 4.25$ represent excellent candidates for a targeted search for AGN within BCDs. A list of the BCDs that WISE colors indicate potential AGN can be seen in Table 2.

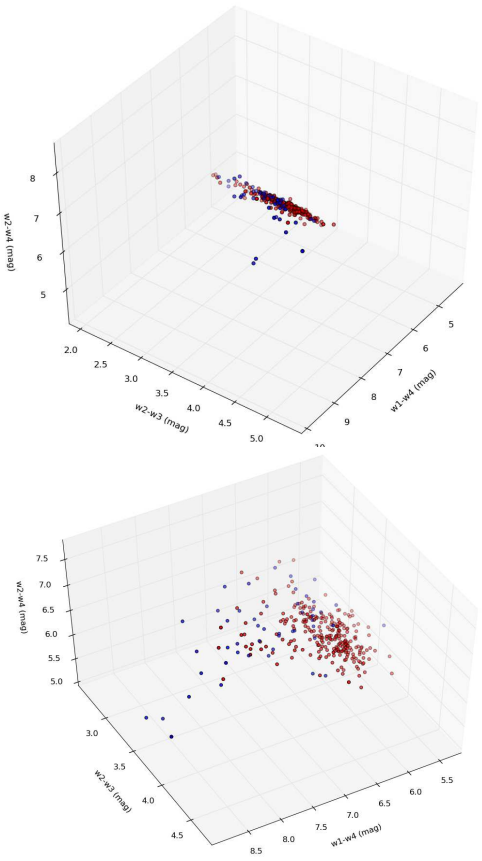

Fig. 2.— Three dimensional plots of WISE mid-infrared colors. The plot at top shows the plane that most BCDs and spirals fall upon. The plot below show the same data, but rotated to show the spread in colors between galaxies. Spiral galaxies are represented by red dots, BCDs detected in NED by blue dots, He 2-10 by a cyan dot, and green dots are BCDs from (Wu et al. 2008; Griffith et al. 2011).

Finding additional BCDs with AGN would be important for constraining models of galaxy formation as well as supermassive black hole development.

Though the search for AGN in dwarf galaxies is not a new concept (Filippenko & Ho 2003), the discovery of the first AGN in a BCD has been relatively recent (Reines et al. 2011). The confirmation of a AGN BCD candidate noted on our previ-

TABLE 2
LIST OF BCDS POTENTIALLY CONTAINING AGN.

Name	RA J2000	Dec J2000	Distance Mpc	W1-W2 [mag]	W1-W3 [mag]	W1-W4 [mag]	W2-W3 [mag]	W2-W4 [mag]	W3-W4 [mag]
W0801+26	08:01:03.9	+26:40:53.9		2.096	6.731	9.719	4.635	7.623	2.988
W1702+18	17:02:33.5	+18:03:06.4		2.219	6.643	9.323	4.424	7.104	2.68
UGCA 166 (I Zw 18)	09:34:02.0	+55:14:26.2		0.611	3.965	7.56	3.354	6.949	3.595
SDSS J0825+3532	08:25:55.5	+35:32:32.0		0.36	4.168	7.934	3.808	7.574	3.766
Holmberg II	08:19:05.0	+70:43:12	3.34	0.493	2.525	6.264	2.032	5.771	3.739
UGCA 412	16:35:21.1	+52:12:53	41	0.176	3.998	7.069	3.822	6.893	3.071
MRK 0709	09:49:18.0	+16:52:44		0.323	4.333	7.541	4.01	7.218	3.208
UGCA 211	10:27:02.0	+56:16:14	15.6	0.181	2.435	5.957	2.254	5.776	3.522
MRK 1450	11:38:35.6	+57:52:27		0.354	4.763	8.361	4.409	8.007	3.598
IC 0691	11:26:44.3	+59:09:20	23.7	0.649	4.538	7.291	3.889	6.642	2.753
He 2-10	08:36:15.1	-26:24:34	10.5	0.422	5.353	8.662	4.931	8.24	3.309
VCC 1313	12:30:48.5	+12:02:42	16.8	0.464	3.41	7.255	2.946	6.791	3.845
UGC 07354	12:19:09.9	+03:51:23	14.6	0.35	5.051	8.4	4.701	8.05	3.349
UM 455	11:50:23.9	-00:31:41		0.332	3.714	7.1	3.382	6.768	3.386
UGCA 296	12:45:36.4	+71:19:07	20.1	0.144	4.177	6.639	4.033	6.495	2.462
UGCA 272	12:07:47.6	+67:23:02	35.4	0.02	3.233	6.454	3.213	6.434	3.221
TOLOLO 0610-387	06:12:14.2	-38:46:23		0.102	3.182	5.657	3.08	5.555	2.475
UGCA 208	10:16:28.2	+45:19:18	27.1	0.115	3.945	6.892	3.83	6.777	2.947
SBS 1147+520	11:49:54.5	+51:44:11		0.211	3.359	5.347	3.148	5.136	1.988
MRK 1426	09:49:18.3	+48:33:50		0.036	2.939	5.177	2.903	5.141	2.238

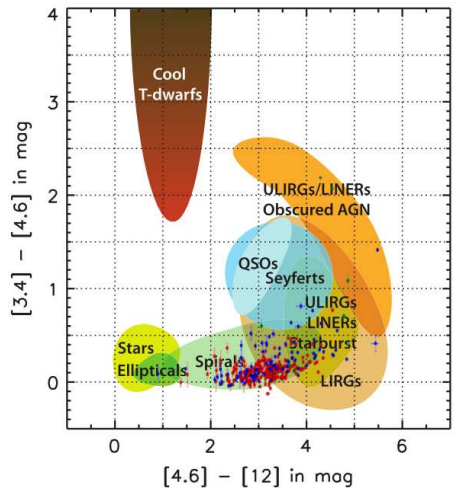

Fig. 3.— An adaptation of Figure 12 taken from Wright et al. (2010). As in previous figures, red points represent spiral galaxies while blue (from NED), cyan (He 2-10), and green (Wu et al. 2008; Griffith et al. 2011) dots represent BCDs. Several BCDs lie within the WISE color range for active galaxies indicated by Wright et al. (2010) and may indicated additional BCDs containing AGN.

ous table can be accomplished through investigation of additional wavelengths for a non-thermal emission source (Reines et al. 2011). Using continuum observations from the Very Large Array at 4.9GHz and 8.5GHz can be used to detect non-thermal emission from an AGN. The Chandra X-ray Observatory could then be used to check to see if there is a Hard X-ray source coincident with a non-thermal radio source. If both a non-thermal radio source and a hard X-ray source are found within the BCDs identified in our study, it would be strong evidence for the presence of an AGN in these galaxies (Reines et al. 2011).

We are grateful to P. Kaaret for the python template code to plot the WISE data and to B. Scheiner for his constructive comments. This research has made use of the NASA/IPAC Extragalactic Database (NED) and the NASA/ IPAC Infrared Science Archive, which are operated by the Jet Propulsion Laboratory, California Institute of Technology, under contract with the National Aeronautics and Space Administration. This publication makes use of data products from the Wide-field Infrared Survey Explorer, which is a joint project of the University of California, Los Angeles, and the Jet Propulsion Laboratory/California Institute of Technology, funded by the National Aeronautics and Space Administration.

Facilities: WISE

REFERENCES

Barth, A. J., Ho, L. C., Rutledge, R. E., & Sargent, W. L. W. 2004, ApJ, 607, 90

Bekki, K. 2008, MNRAS, 388, L10

Cairós, L. M., Caon, N., Zurita, C., et al. 2010, A&A, 520, A90

Filippenko, A. V., & Ho, L. C. 2003, ApJ, 588, L13

Filippenko, A. V., & Sargent, W. L. W. 1989, ApJ, 342, L11

Gil de Paz, A., Madore, B. F., & Pevunova, O. 2003, ApJS, 147, 29

Griffith, R. L., Tsai, C.-W., Stern, D., et al. 2011, ApJ, 736, L22

Izotov, Y. I., & Thuan, T. X. 1999, ApJ, 511, 639

Kunth, D., & Östlin, G. 2000, A&A Rev., 10, 1

Olive, K. A., Schramm, D. N., Steigman, G., & Walker, T. P. 1990, Physics Letters B, 236, 454

Reines, A. E., Sivakoff, G. R., Johnson, K. E., & Brogan, C. L. 2011, Nature, 470, 66

Sánchez Almeida, J., Muñoz-Tuñón, C., Amorín, R., et al. 2008, ApJ, 685, 194

Searle, L., & Sargent, W. L. W. 1972, ApJ, 173, 25

Wright, E. L., Eisenhardt, P. R. M., Mainzer, A. K., et al. 2010, AJ, 140, 1868

Wu, Y., Bernard-Salas, J., Charmandaris, V., et al. 2008, ApJ, 673, 193

Zhao, Y., Gu, Q., & Gao, Y. 2011, AJ, 141, 68

This 2-column preprint was prepared with the AAS LaTeX macros v5.2.

Table 3
WISE Detected BCDs

WISE Designation	RA J2000	Dec J2000	W1-W2 [mag]	W1-W3 [mag]	W1-W4 [mag]	W2-W3 [mag]	W2-W4 [mag]	W3-W4 [mag]
J002017.23+591813.4	00h20m17.3s	+59d18m14s	0.057	2.621	6.172	2.564	6.115	3.551
J003203.13+180446.7	00h32m03.1s	+18d04m46s	0.326	4.234	7.716	3.908	7.39	3.482
J004546.44-153548.5	00h45m46.4s	-15d35m49s	-0.007	3.054	5.805	3.061	5.812	2.751
J005158.76-014018.0	00h51m58.7s	-01d40m19s	0.439	3.715	6.629	3.276	6.19	2.914
J005159.62-002911.9	00h51m59.6s	-00d29m12s	-0.004	2.96	4.851	2.964	4.855	1.891
J012646.54-003845.0	01h26m46.6s	-00d38m46s	0.142	2.757	6.713	2.615	6.571	3.956
J012735.51-061935.4	01h27m35.5s	-06d19m36s	0.402	3.85	7.096	3.448	6.694	3.246
J014441.36+045327.9	01h44m41.3s	+04d53m26s	0.423	3.866	7.636	3.443	7.213	3.77
J015809.45-000639.4	01h58m09.4s	-00d06m38s	0.434	4.173	7.262	3.739	6.828	3.089
J021012.07-012451.0	02h10m12.0s	-01d24m52s	0.693	4.248	8.177	3.555	7.484	3.929
J021123.44+022030.1	02h11m23.4s	+02d20m30s	0.267	3.258	7.092	2.991	6.825	3.834
J021930.28-005911.4	02h19m30.3s	-00d59m11s	0.55	4.954	8.578	4.404	8.028	3.624
J024028.98+191749.7	02h40m29.0s	+19d17m50s	0.142	3.776	6.653	3.634	6.511	2.877
J025104.71+042712.2	02h51m04.6s	+04d27m14s	0.394	3.641	7.652	3.247	7.258	4.011
J033929.62-352651.6	03h39m29.6s	-35d26m52s	-0.038	3.907	8.059	3.945	8.097	4.152
J040607.85-524008.4	04h06m07.9s	-52d40m06s	0.148	3.661	7.322	3.513	7.174	3.661
J045413.50-532139.7	04h54m13.5s	-53d21m40s	0.144	2.128	4.721	1.984	4.577	2.593
J051045.34-024528.4	05h10m45.3s	-02d45m31s	0.137	3.923	7.824	3.786	7.687	3.901
J051048.10-024053.8	05h10m48.1s	-02d40m54s	0.071	3.287	6.45	3.216	6.379	3.163
J055542.61+032331.8	05h55m42.6s	+03d23m32s	1.431	6.886	10.057	5.455	8.626	3.171
J061214.17-384623.5	06h12m14.2s	-38d46m23s	0.102	3.182	5.657	3.08	5.555	2.475
J064215.49+753731.7	06h42m15.5s	+75d37m33s	0.308	3.991	7.258	3.683	6.95	3.267
J072811.60+723425.8	07h28m11.5s	+72d34m23s	0.026	3.56	6.278	3.534	6.252	2.718
J075614.19+601814.6	07h56m14.2s	+60d18m15s	0.491	3.985	6.631	3.494	6.14	2.646
J081314.68+455924.4	08h13m14.6s	+45d59m23s	0.008	2.649	5.002	2.641	4.994	2.353
J082555.51+353232.9	08h25m55.5s	+35d32m32s	0.36	4.168	7.934	3.808	7.574	3.766
J085315.60+731119.9	08h53m15.6s	+73d11m20s	0.15	3.892	6.198	3.742	6.048	2.306
J085829.85+061916.4	08h58m29.8s	+06d19m17s	0.242	4.211	7.206	3.969	6.964	2.995
J092055.92+523407.0	09h20m56.0s	+52d34m08s	0.526	4.095	7.874	3.569	7.348	3.779
J092130.11+641419.5	09h21m30.1s	+64d14m19s	0.258	4.167	7.707	3.909	7.449	3.54
J092601.16+192300.1	09h26m01.2s	+19d23m01s	0.292	4.625	7.205	4.333	6.913	2.58
J094026.98+482015.6	09h40m27.0s	+48d20m15s	-0.039	2.72	5.797	2.759	5.836	3.077
J094301.68+585825.0	09h43m01.6s	+58d58m25s	0.061	3.279	5.659	3.218	5.598	2.38
J094416.79+541133.7	09h44m16.6s	+54d11m34s	0.825	4.892	8.315	4.067	7.49	3.423
J094705.78+540539.4	09h47m05.8s	+54d05m40s	0.18	3.336	6.809	3.156	6.629	3.473
J094747.64+390503.8	09h47m47.6s	+39d05m03s	0.031	2.544	5.73	2.513	5.699	3.186
J094804.71+325257.1	09h48m04.7s	+32d52m57s	0.018	3.327	6.093	3.309	6.075	2.766
J094918.01+165244.9	09h49m18.0s	+16d52m44s	0.323	4.333	7.541	4.01	7.218	3.208
J094918.35+483350.0	09h49m18.3s	+48d33m50s	0.036	2.939	5.177	2.903	5.141	2.238
J094930.48+553448.6	09h49m30.3s	+55d34m47s	0.365	4.047	7.658	3.682	7.293	3.611
J094941.20+321315.9	09h49m41.2s	+32d13m16s	-0.02	2.591	4.677	2.611	4.697	2.086
J095614.80-293619.4	09h56m14.8s	-29d36m19s	0.145	3.649	6.443	3.504	6.298	2.794
J095921.21-280801.4	09h59m21.2s	-28d08m00s	0.139	3.418	7.382	3.279	7.243	3.964
J100633.38-295607.5	10h06m33.4s	-29d56m05s	0.301	4.943	8.327	4.642	8.026	3.384
J100935.37+573401.0	10h09m35.3s	+57d34m00s	0.027	1.827	5.732	1.8	5.705	3.905
J101457.11+595111.8	10h14m57.1s	+59d51m12s	0.06	2.272	6.21	2.212	6.15	3.938
J101459.22+594903.2	10h14m59.1s	+59d49m03s	0.103	3.067	6.67	2.964	6.567	3.603
J101628.25+451917.9	10h16m28.2s	+45d19m18s	0.115	3.945	6.892	3.83	6.777	2.947
J103231.92+542403.0	10h32m32.0s	+54d24m02s	0.289	4.949	8.178	4.66	7.889	3.229
J103410.18+580349.4	10h34m10.2s	+58d03m49s	0.529	3.698	7.618	3.169	7.089	3.92

TABLE 3—*Continued*

WISE Designation	RA J2000	Dec J2000	W1-W2 [mag]	W1-W3 [mag]	W1-W4 [mag]	W2-W3 [mag]	W2-W4 [mag]	W3-W4 [mag]
J104109.61+212143.3	10h41m09.6s	+21d21m43s	0.437	4.386	8.011	3.949	7.574	3.625
J105308.07+335436.8	10h53m08.1s	+33d54m37s	0.182	4.358	6.486	4.176	6.304	2.128
J105308.55+501704.3	10h53m08.4s	+50d17m05s	0.206	1.945	6.111	1.739	5.905	4.166
J105658.71+500826.2	10h56m58.7s	+50d08m26s	0.065	3.309	5.822	3.244	5.757	2.513
J111705.54+583100.0	11h17m05.5s	+58d31m00s	0.073	3.13	5.862	3.057	5.789	2.732
J111934.27+513011.9	11h19m34.4s	+51d30m12s	0.319	2.688	6.873	2.369	6.554	4.185
J112141.60+573530.0	11h21m41.6s	+57d35m30s	0.085	2.838	5.443	2.753	5.358	2.605
J112612.97+572112.4	11h26m12.9s	+57d21m13s	0.071	3.254	6.294	3.183	6.223	3.04
J112732.70+535454.9	11h27m32.7s	+53d54m54s	0.418	4.211	7.66	3.793	7.242	3.449
J113835.69+575227.3	11h38m35.7s	+57d52m27s	0.354	4.763	8.361	4.409	8.007	3.598
J114032.07+583832.2	11h40m32.1s	+58d38m32s	-0.071	3.322	6.906	3.393	6.977	3.584
J114700.69-001738.7	11h47m00.7s	-00d17m39s	0.071	2.708	5.289	2.637	5.218	2.581
J114954.45+514411.3	11h49m54.5s	+51d44m11s	0.211	3.359	5.347	3.148	5.136	1.988
J115003.18-284016.8	11h50m03.2s	-28d40m17s	0.2	3.651	6.644	3.451	6.444	2.993
J115023.80-003141.5	11h50m23.9s	-00d31m41s	0.332	3.714	7.1	3.382	6.768	3.386
J115036.28-003405.7	11h50m36.3s	-00d34m03s	0.203	3.718	7.569	3.515	7.366	3.851
J115050.05+481504.9	11h50m50.0s	+48d15m05s	0.398	3.389	6.478	2.991	6.08	3.089
J115227.38+345340.1	11h52m27.4s	+34d53m40s	0.139	3.87	6.818	3.731	6.679	2.948
J115728.05-193726.5	11h57m28.0s	-19d37m27s	0.217	4.066	7.391	3.849	7.174	3.325
J120747.64+672301.8	12h07m47.6s	+67d23m02s	0.02	3.233	6.454	3.213	6.434	3.221
J120820.38+134059.9	12h08m20.3s	+13d41m02s	0.13	3.224	5.44	3.094	5.31	2.216
J120828.23+552526.5	12h08m28.2s	+55d25m26s	0.225	3.767	6.971	3.542	6.746	3.204
J121214.72+000420.4	12h12m14.7s	+00d04m20s	0.047	2.168	5.683	2.121	5.636	3.515
J121402.50+534518.4	12h14m02.5s	+53d45m17s	0.217	3.502	7.273	3.285	7.056	3.771
J121503.98+094512.7	12h15m04.0s	+09d45m13s	-0.077	2.717	6.689	2.794	6.766	3.972
J121909.87+035122.9	12h19m09.9s	+03d51m23s	0.35	5.051	8.4	4.701	8.05	3.349
J121953.18+014624.4	12h19m53.2s	+01d46m24s	0.069	3.23	5.817	3.161	5.748	2.587
J121959.51-172330.9	12h19m59.5s	-17d23m31s	0.26	4.574	7.452	4.314	7.192	2.878
J122111.24+173818.4	12h21m11.3s	+17d38m19s	0.051	2.688	5.007	2.637	4.956	2.319
J122337.55+173228.6	12h23m37.5s	+17d32m27s	0.061	3.24	5.588	3.179	5.527	2.348
J122417.04+672623.8	12h24m17.0s	+67d26m24s	0.33	4.812	7.954	4.482	7.624	3.142
J122542.80+003421.5	12h25m42.8s	+00d34m21s	0.25	5.148	8.379	4.898	8.129	3.231
J122547.52+145708.1	12h25m47.5s	+14d57m07s	0.176	3.743	6.27	3.567	6.094	2.527
J122552.55+054836.0	12h25m52.5s	+05d48m35s	0.159	2.714	5.613	2.555	5.454	2.899
J122615.82+482938.5	12h26m15.9s	+48d29m37s	0.635	5.071	8.817	4.436	8.182	3.746
J123048.52+120242.4	12h30m48.5s	+12d02m42s	0.464	3.41	7.255	2.946	6.791	3.845
J123815.51+065939.3	12h38m15.5s	+06d59m39s	0.34	2.423	6.111	2.083	5.771	3.688
J124517.09+270731.5	12h45m17.1s	+27d07m31s	0.181	3.777	7.065	3.596	6.884	3.288
J124536.45+711907.3	12h45m36.4s	+71d19m07s	0.144	4.177	6.639	4.033	6.495	2.462
J131448.45+345252.1	13h14m48.3s	+34d52m51s	0.135	3.238	5.704	3.103	5.569	2.466
J131649.69+601833.4	13h16m49.7s	+60d18m33s	0.101	2.737	6.223	2.636	6.122	3.486
J131652.35+123254.0	13h16m52.3s	+12d32m54s	-0.028	2.781	5.668	2.809	5.696	2.887
J131922.14-150923.2	13h19m22.2s	-15d09m24s	0.124	3.666	5.649	3.542	5.525	1.983
J132548.63-113637.9	13h25m48.7s	-11d36m38s	0.419	5.841	9.28	5.422	8.861	3.439
J133305.94+685137.7	13h33m05.9s	+68d51m38s	0.101	3.408	6.161	3.307	6.06	2.753
J134156.48+303109.8	13h41m56.5s	+30d31m10s	0.459	4.767	8.129	4.308	7.67	3.362
J134251.82+524230.8	13h42m51.8s	+52d42m31s	0.17	3.342	6.787	3.172	6.617	3.445
J134259.47+524117.5	13h42m59.4s	+52d41m18s	0.311	3.025	6.907	2.714	6.596	3.882
J134822.32-422114.1	13h48m22.3s	-42d21m15s	0.277	3.885	7.432	3.608	7.155	3.547
J140236.11+391312.9	14h02m36.1s	+39d13m13s	0.077	3.327	6.971	3.25	6.894	3.644

TABLE 3—*Continued*

WISE Designation	RA J2000	Dec J2000	W1-W2 [mag]	W1-W3 [mag]	W1-W4 [mag]	W2-W3 [mag]	W2-W4 [mag]	W3-W4 [mag]
J141701.44+433006.1	14h17m01.4s	+43d30m05s	0.647	4.539	8.538	3.892	7.891	3.999
J143012.16+453230.6	14h30m12.2s	+45d32m32s	0.23	4.065	7.581	3.835	7.351	3.516
J143905.47+364821.1	14h39m05.5s	+36d48m22s	0.425	3.791	7.247	3.366	6.822	3.456
J144215.98+424949.2	14h42m16.0s	+42d49m50s	0.312	4.609	7.833	4.297	7.521	3.224
J144412.73+423743.3	14h44m12.8s	+42d37m44s	0.259	2.74	6.322	2.481	6.063	3.582
J144738.94+592151.9	14h47m38.9s	+59d21m52s	0.056	1.914	5.884	1.858	5.828	3.97
J145022.74+112411.0	14h50m22.7s	+11d24m11s	0.128	3.38	6.481	3.252	6.353	3.101
J145056.55+353418.6	14h50m56.5s	+35d34m18s	0.267	4.18	7.916	3.913	7.649	3.736
J145114.43+353232.2	14h51m14.4s	+35d32m32s	0.011	3.019	5.545	3.008	5.534	2.526
J145439.10+420125.2	14h54m39.3s	+42d01m26s	0.074	4.098	7.096	4.024	7.022	2.998
J153704.19+551549.8	15h37m04.2s	+55d15m48s	0.777	5.059	8.278	4.282	7.501	3.219
J161111.49+482004.1	16h11m11.5s	+48d20m04s	0.063	2.994	5.673	2.931	5.61	2.679
J161517.03+130133.1	16h15m17.0s	+13d01m33s	0.604	4.626	8.348	4.022	7.744	3.722
J163521.05+521252.3	16h35m21.0s	+52d12m52s	0.176	3.998	7.069	3.822	6.893	3.071
J191641.27+635822.3	19h16m41.1s	+63d58m24s	0.09	1.573	4.664	1.483	4.574	3.091
J192758.00-413431.6	19h27m58.2s	-41d34m32s	0.558	5.284	8.837	4.726	8.279	3.553
J194058.64-421544.7	19h40m58.6s	-42d15m45s	0.045	3.27	5.563	3.225	5.518	2.293
J212959.64+022451.7	21h29m59.6s	+02d24m51s	0.072	3.33	6.008	3.258	5.936	2.678
J230259.19+163616.5	23h02m59.3s	+16d36m19s	0.16	3.788	7.321	3.628	7.161	3.533
J232632.71+181601.8	23h26m32.8s	+18d16m00s	0.068	1.536	5.705	1.468	5.637	4.169
J232632.82+181557.3	23h26m32.8s	+18d16m00s	-0.046	1.677	5.106	1.723	5.152	3.429
J233739.57+300746.6	23h37m39.6s	+30d07m46s	0.087	3.489	5.947	3.402	5.86	2.458